Linear phase shift electrodes for the planar electrooptic prism deflector

Chung Len Lee, Jyh Fa Lee, and Juang Yau Huang

Three types of compensation electrode are analyzed, which give a more linear phase shift to the propagating optical beam for the planar electrooptic prism deflector. For Types I and III, the more linear phase shift is achieved by varying the slope of the central tilt electrode at the edge regions. For Type II, the more linear phase shift is achieved by cascading an electrode, giving an opposite phase shift to the conventional electrode at the edge regions. Theoretically, Type III is expected to perform best. A physical device was made with Type III electrodes in an array, and it has shown significant improvement in sidelobe suppression and beam size conservation.

I. Introduction

In integrated optics, various kinds of devices have been invented and demonstrated as optical modulators, switches, and deflectors.[1–4] Among these there is a planar electrooptic deflector of simulated prism structure[5] that achieves optical deflection by arranging the electrode in a prism fashion [Fig. 1(a)], thus creating an approximately linear phase shift via the electrooptic effect on the width of the propagating optical beam. It has also been designed in arrays as an optical beam deflector[6] and beam splitter[7] with enhanced spot resolution power.

One drawback of this simulated planar electrooptic prism is that the phase shift created by the electrode, although it is approximately linear at the center region of the aperture of the device, is steeper at both edges.[5] This nonlinear phase shift deteriorates the propagating beam spot quality when the device is used singly and causes cross talk due to sidelobes when it is used in arrays.[7] To reduce this effect, a dogleg [Fig. 1(b)] electrode configuration was introduced by Bulmer *et al.*[8] where the slope of the central tilt electrode was changed at the two edge regions. Changing the electrode slope gives a smaller electric field at the edge regions thus reducing the over-phase-shift. However, since that paper[8] emphasizes on assessing capabilities and properties of the general electrooptic waveguide array deflectors, no detailed theoretical study or experimental data was presented concerning the phase shift of that type of electrode.

The authors are with National Chiao Tung University, Institute of Electronics, Hsin-Chu, Taiwan, China.

Received 26 March 1980.
0003-6935/80/172902-04$00.50/0.

This paper theoretically studies the dogleg and two other types of electrode. Deflection angle θ in terms of incident beam height z is derived and plotted across the aperture for each type of electrode. An experimental planar deflector is realized with one type of electrode which is theoretically predicted to give the best performance. Test results shwo that significant improvements in output beam spot quality are obtained.

II. Theoretical Analysis

The types of compensation electrode studied are shown in Fig. 1 with the conventional electrode, together with the nomenclature and coordinate system. The devices are assumed to be realized on a Y-cut X-propagation $LiNbO_3$ crystal. In the analysis, the Kaminow and Stulz[5] approach is used. The applied electric field distribution is assumed uniform in the y direction in the waveguide. For the conventional electrode configuration [Fig. 1(a)], the electric field can be expressed as[5]

$$E_z(x,z) = -\frac{V_0}{\pi}[z(d-z)]^{-1/2} \quad \text{for } 0 < z < d$$
$$= \frac{V_0}{\pi}[(A-z)(z-d)]^{-1/2} \quad \text{for } d < z < A,$$

where $d = z_0 + ax$,
a = the slope of the central tilt electrode,
V_0 = the applied voltage, and
A = the aperture of the electrode.

To analyze the electrodes of Figs. 1(b), (c), and (d), the same expressions are used except that slope a is given different values for various regions of each device. The phase shift in terms of the incident beam height is obtained by integrating the induced eo refractive-index change through the whole device length, i.e.,

$$\eta(z) = \frac{2\pi}{\lambda}\int_0^B \Delta n dx,$$

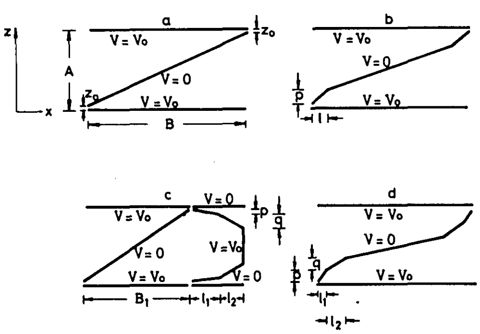

Fig. 1. Electrode configurations for planar prism electrooptic deflectors: (a) conventional; (b) Type I (dogleg); (c) Type II; and (d) Type III.

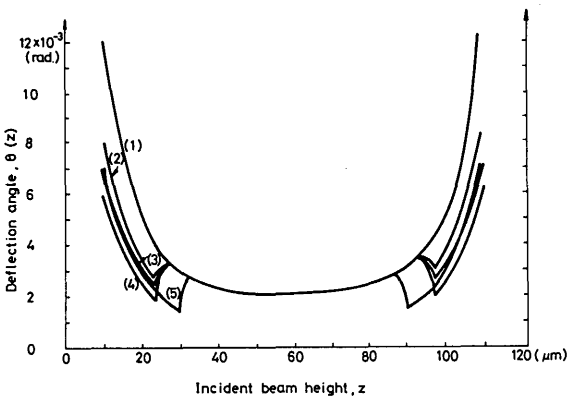

Fig. 2. Calculated deflection curves $\theta(z)$ for the conventional and Type I electrodes: curve (1), conventional; curves (2), (3), (4), and (5), Type I where $p = 14\ \mu$m, $l = 570\ \mu$m; $p = 14\ \mu$m, $l = 500\ \mu$m; $p = 14\ \mu$m, $l = 430\ \mu$m; and $p = 20\ \mu$m, $l = 710\ \mu$m, respectively. For all the electrodes, $A = 120\ \mu$m, $B = 6000\ \mu$m, and $z_0 = 10\ \mu$m, and the applied voltage is 30 V.

where λ = the wavelength of light,
B = the length of the electrode,
$\Delta n = n_e^3\gamma_{33}E_z/2$, and
n_e, γ_{33} = the extraordinary index of refraction and the appropriate eo constant of the $LiNbO_3$ crystal.

To express the degree of deflection for different incident beam heights, the deflection angle, $\theta(z)$ $(= (\lambda/2\pi n_e)[d\eta(z)/dz])$, is plotted instead of the phase shift. This gives a direct indication of how the beam is deflected across the width of the electrode.

A. Type I Electrode [Fig. 1(b)]

This is the dogleg electrode introduced by Bulmer *et al.*[8] The electrode pattern is basically the same as the conventional type except that the slope of the central tilt electrode is changed at two edge regions. To analyze this electrode, a piecewise approach is used, i.e., the electrode is divided into three regions. For each region, deflection angle $\theta(z)$ is derived as

$$\theta(z) = \frac{n_e^2\gamma_{33}V_0}{2\pi a}\left\{\frac{1}{[(z-z_0)(A-z)]^{1/2}} + \frac{(z-z_0)^{1/2}}{(A-z)^{3/2}} + \frac{1}{[(A-z-z_0)z]^{1/2}} + \frac{(A-z-z_0)^{1/2}}{z^{3/2}}\right\}.$$

For regions $z_0 < z < p + z_0$ and $A - z_0 - p < z < A - z_0$, $a = a_1 = p/l$; for region $p + z_0 < z < A - z_0 - p$, $a = a_2 = (A - 2z_0 - 2p)/(B - 2l)$. In the above, a_1 is assumed to be greater than a_2 so that a steeper slope is obtained on the edge region of the electrode. The above expression is plotted in Fig. 2 for several sets of values of p and l. For comparison, the deflection curve for a conventional electrode of similar dimensions is also plotted. For the deflection curves in Fig. 2, it is necessary for the curves to be constant throughout the aperture of the electrode. It can be seen that, compared with the conventional type of electrode, improvements are obtained at the edge regions. It is noted that the value of p determines the position of the dips of the curve. To achieve desirable compensation, p in general should be small, but too small a value will increase the bumps in the curves. It is also noted that the value of l determines the degree of compensation; the smaller l is, the more compensation is obtained. To get good compensation, an appropriate value for l should be chosen. In the figure l is 430 μm for curve (4) giving the most linear deflection.

B. Type II Electrode [Fig. 1(c)]

The basic idea for this type of electrode is that an additional compensation electrode producing a phase shift in the opposite direction is cascaded behind the conventional electrode to compensate the overall phase shift at the edge regions. The analysis of this electrode is similar to Type I except that in calculating the phase shift, integration boundary B extends to the end of the cascading electrode. Deflection angle $\theta(z)$ is derived as

$$\theta(z) = \frac{n_e^2\gamma_{33}V_0}{2\pi}\left\{\frac{1}{a_1[(z-z_0)(A-z)]^{1/2}} + \frac{(z-z_0)^{1/2}}{a_1(A-z)^{3/2}} + \frac{1}{a_1[z(A-z-z_0)]^{1/2}} + \frac{(A-z-z_0)^{1/2}}{a_1 z^{3/2}} - \frac{1}{a_2(z|p+z_0-z|)^{1/2}} - \frac{|p+z_0-z|^{1/2}}{a_2 z^{3/2}}\right\}$$

for regions $z_0 < z < p + z_0$ and $A - p - z_0 < z < A - z_0$, where $a_1 = (A - 2z_0)/B_1$ and $a_2 = p/l_1$. For regions $p + z_0 < z < q + p + z_0$ and $A - p - q - z_0 < z < A - p - z_0$, the expression for $\theta(z)$ is the same as above except that a_2 is substituted by a_3, where $a_3 = q/l_2$. For region $p + q + z_0 < z < A - p - q - z_0$, since there is no compensation, the expression for $\theta(z)$ is also the same as the above except the terms containing a_2 are missing.

The above expression is plotted in Fig. 3 for several sets of different values of p, q, l_1, and l_2. The deflection angle for the uncompensated conventional electrode is also included. It can be seen that compensation for this type of electrode is better than it is for Type I. Since there are two slopes on the compensating electrode at the edge region, two dips appear at each edge of the

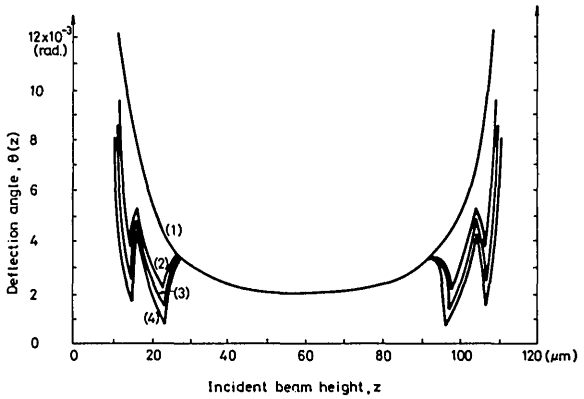

Fig. 3. Calculated deflection curves $\theta(z)$ for the conventional and Type II electrodes: curve (1), conventional; curves (2), (3), and (4), Type II where $l_1 = 150\ \mu$m, $l_2 = 160\ \mu$m; $l_1 = 210\ \mu$m, $l_2 = 200\ \mu$m; and $l_1 = 240\ \mu$m, $l_2 = 240\ \mu$m, respectively, and $p = 6\ \mu$m, $q = 8\ \mu$m. For all the electrodes, $A = 120\ \mu$m, $B = 6000\ \mu$m, and $z_0 = 10\ \mu$m, and the applied voltage is 30 V.

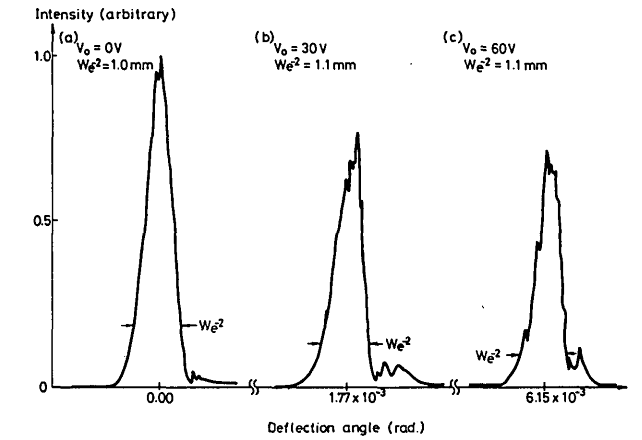

Fig. 5. Spot profiles of the output beams of the prism deflector fabricated with a Type III electrode with applied voltages of 0, 30, and 60 V, respectively. The theoretically calculated deflection angles of the center of the beams are 0.00, 1.49×10^{-3}, and 2.98×10^{-3} rad, respectively.

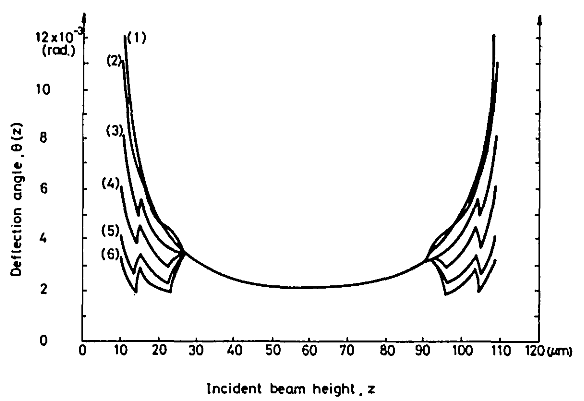

Fig. 4. Calculated deflection curves $\theta(z)$ for the conventional and Type III electrodes: curve (1), conventional; curves (2), (3), (4), (5), and (6), Type III where $l_1 = 90\ \mu$m, $l_2 = 200\ \mu$m; $l_1 = 120\ \mu$m, $l_2 = 240\ \mu$m; $l_1 = 180\ \mu$m, $l_2 = 320\ \mu$m; $l_1 = 240\ \mu$m, $l_2 = 400\ \mu$m; and $l_1 = 330\ \mu$m, $l_2 = 480\ \mu$m, respectively, and $p = 6\ \mu$m, $q = 8\ \mu$m. For all the electrodes, $A = 120\ \mu$m, $B = 6000\ \mu$m, and $z_0 = 10\ \mu$m, and the applied voltage is 30 V.

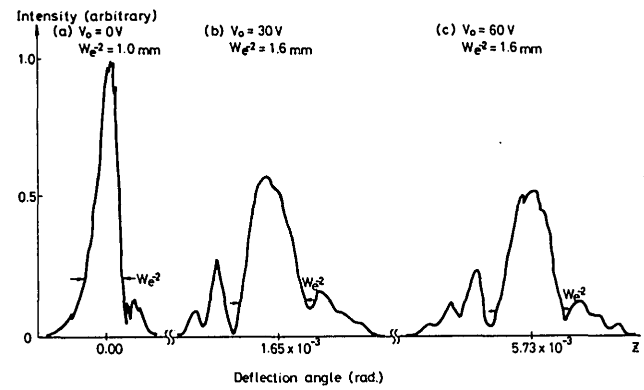

Fig. 6. Spot profiles of the output beams of the prism deflector fabricated with a conventional electrode with applied voltages of 0, 30, and 60 V, respectively. The theoretically calculated deflection angles of the center of the beams are 0.00, 1.25×10^{-3}, and 2.50×10^{-3} rad, respectively.

deflection curves. The positions of the dips are determined by the values of p and q. Similarly, the degree of compensation is determined by l_1 and l_2. By choosing an appropriate combination, good compensation can be obtained.

C. Type III Electrode [Fig. 1(d)]

According to the above analysis, one breakpoint on the slope of the central tilt electrode corresponds to one dip in the deflection curve. More dips in the deflection curve and, consequently, better compensation can be achieved by breaking the central tilt electrode into more slopes. The Type III electrode is based on this idea, where the central tilt electrode is broken into one more slope at the edge region. The expression for deflection angle $\theta(z)$ is the same as that of Type I except that, for regions $z_0 < z < p + z_0$ and $A - p - z_0 < z < A - z_0$, electrode slope a is equal to p/l_1, for regions $p + z_0 < z < p + q + z_0$ and $A - p - q - z_0 < z < A - p - z_0$, a is equal to g/l_2, and for region $p + q + z_0 < z < A - p - q - z_0$, a is equal to $(A - 2z_0 - 2p - 2q)/(B - 2l_1 - 2l_2)$.

The deflection curves are plotted in Fig. 4. It can be seen that a much better compensation can be obtained for this type of electrode [e.g., curve (6)]. If the breaking point at the central tilt electrode is designed to be round, an even better result can be expected.

III. Experiments

The compensation effect from the above analysis was then experimentally demonstrated. Two prism deflectors were realized by designing one Type III electrode with round breaking points and the other a conventional electrode. Both devices were designed in arrays and fabricated on out-diffused $LiNbO_3$ planar waveguides. A He–Ne laser beam was coupled into each device and deflected. The effect of compensation is observed by examining the spot patterns of the deflected output beams. Figure 5 shows the output beam profiles for a Type III electrode with applied voltages of 0, 30, and 60 V. These profiles can be compared with Fig. 6 where the output beam profiles are plotted for a conventional electrode in similar conditions. For the conventional device, significant sidelobes are observed for profiles for 30 and 60 V. This is due to the incomplete suppression of the sidelobes of each neighboring electrode since each one produces a nonlinear phase shift. For the compensated Type III, a significant improvement is obtained, and an improvement of the deflected beam size is also obtained. For the conventional electrode, waist $W_{e^{-2}}$ of the deflected beam expands from 1.0 (arbitrary unit) to 1.6, while for Type III, it only expands to 1.1.

The values of the parameters for these two devices are $B = 3250\ \mu m$, $A = 120\ \mu m$, $l_1 = 120\ \mu m$, $l_2 = 240\ \mu m$, $p = 6\ \mu m$, $q = 8\ \mu m$, and $z_0 = 10\ \mu m$ for Type III, and $B = 3250\ \mu m$, $A = 120\ \mu m$, and $z_0 = 10\ \mu m$ for the conventional electrode. For both devices the electrode width is 10 μm, and the number of electrodes is twelve in each array.

IV. Conclusions

Three types of compensation electrode for the planar eo prism deflector have been analyzed. All types of electrode are theoretically shown to exhibit a more linear phase shift at the edge regions than does the conventional device to the propagating optical beam. For Type I (the so-called dogleg) and Type III, compensation is achieved by varying the slope of the central tilt electrode at the edge regions. For Type II, compensation is achieved by cascading an electrode giving an opposite phase shift to that of the conventional device. Of the three, Type III is theoretically expected to perform best. Experimentally, a planar eo prism array deflector has been realized with Type III electrodes, and its output beam profiles have shown significant improvement on sidelobe suppression and beam size conservation.

The authors are grateful to the Semiconductor Research Laboratory of NCTU for providing the facilities for fabricating the experimental devices. Financial support from the National Science Council, R.O.C., is also appreciated.

References

1. H. Kogelnik, IEEE Trans. Microwave Theory Tech. **MTT-23,** 2 (1975).
2. E. M. Conwell, Phys. Today **29,** 48 (1976).
3. P. K. Tien, Rev. Mod. Phys. **49,** 361 (1977).
4. See, for example, Trans. IECE Jpn. **61,** special issue on Integrated Optics and Optical Fiber Communication (1978).
5. I. P. Kaminow and L. W. Stulz, IEEE J. Quantum Electron. **QE-11,** 633 (1975).
6. C. S. Tsai and P. Saunier, Appl. Phys. Lett. **27,** 248 (1975).
7. J. Y. Huang and C. L. Lee, Appl. Phys. Lett. **36,** 507 (1980).
8. C. H. Bulmer, W. K. Burns, and T. G. Giallorenzi, Appl. Opt. **18,** 3282 (1979).